Energy Absorption Properties of Periodic and Stochastic 3D Lattice Materials

Jochen Mueller, Kathryn H. Matlack, Kristina Shea, and Chiara Daraio**

Architected lattices can be designed to have tailorable functionalities by controlling their constitutive elements. However, little work has been devoted to comparing energy absorption properties in different periodic three-dimensional geometries to each other and to comparable foam-like random structures. This knowledge is essential for the entire design process. In this work, the authors conduct a systematic and comprehensive computational study of the quasi-static and dynamic energy absorption properties of various different geometries. They test compression loading over strain rates varying from 1 to 10^4 s^{-1}. The authors analyze geometries with varying degrees of nodal connectivity, ranging from bending dominated to stretching dominated, at different orientations, and compare their response to equivalent stochastic lattices. Results show relatively high stress peaks in the periodic lattices, even in bending dominated lattices at certain orientations. Conversely, the stochastic geometries show a relatively constant stress response over large strains, which is ideal for energy absorbing applications. Still, results show that specific orientations of bending dominated periodic lattice geometries outperform their stochastic equivalents. This work can help to quickly identify the potential of different unit cell types and aid in the development of lattices for impulse mitigation applications, such as in protective sports equipment, automotive crashworthiness, and packaging.

1. Introduction

The prospect of using lattice materials for lightweight, multifunctional structures holds promise for many engineering applications, such as the automotive, aerospace, biomedical, and safety equipment. Since the mechanical response of lattices can be controlled with geometric variations of their structure, they offer the ability to engineer specific properties such as stiffness, strength, energy absorption, vibration mitigation, and thermal conductivity directly into the material. New additive manufacturing techniques allow the fabrication of increasingly smaller, more complex, and multi-material structures, accelerating the ability to bring lattice materials to commercialization.

Lattice materials are of particular interest in energy-absorbing applications, such as crashworthiness of vehicles or in protective sport and military equipment, because they can be engineered to control and minimize peak stress during a crushing event.[1] During a high strain-rate event, such as an impact or crash, these materials aim to decrease the peak stress transmitted through the material to a more sensitive region and evenly distribute this stress over a wide range of strains until the material has densified.[2] While much prior work has studied how to engineer lattice materials for enhanced energy absorption properties, most applications primarily use stochastic foams to achieve these functions, which, due to their random structure, are not optimized and are difficult to simulate. Individual works have studied the benefits of engineered periodic structures compared to those of random foams in 2D.[3–5] However, a comprehensive comparison of energy absorbing properties from periodic to stochastic structures in 3D cellular materials remains missing. This is necessary for the categorization and quantitative comparison of existing and new unit cell designs (such as buckling, negative stiffness, and multi-stable unit cells), and serves as a future benchmark for new unit cell designs.

Previous research in the field of energy absorbing lattices focuses predominantly on 2D honeycomb structures, due to their simpler analytical and numerical models,[3,6–13] with fewer studies available for 3D structures.[14–19] Some articles report discrepancies on individual aspects between 2D and 3D structures of the same unit cell type, suggesting that results are not simply scalable and cannot be generalized.[3,6,8,9,16,17,20] For simplicity or due to computational limitations, many studies focus on linear-elastic material properties or deformations in the linear-elastic regime,[6,8–10,16,17] and do not take larger deformations

Dr. J. Mueller, Prof. K. Shea
Engineering Design and Computing Laboratory
Department of Mechanical and Process Engineering
ETH Zurich
8092 Zurich, Switzerland
E-mail: kshea@ehtz.ch
Prof. K. H. Matlack
Wave Propagation and Metamaterials Laboratory
Department of Mechanical Science and Engineering
University of Illinois at Urbana-Champaign
Urbana, IL 61801, USA
Prof. C. Daraio
Division of Engineering and Applied Science
California Institute of Technology
Pasadena, CA 91125, USA
E-mail: daraio@caltech.edu

The ORCID identification number(s) for the author(s) of this article can be found under https://doi.org/10.1002/adts.201900081

DOI: 10.1002/adts.201900081

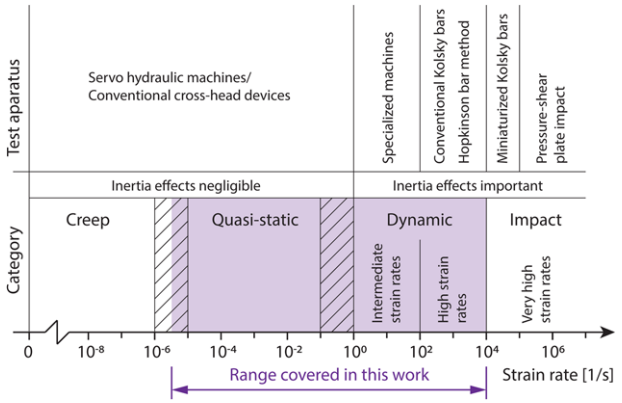

Figure 1. Strain rate ranges and typical applications. Strain rates from approximately zero to $10^6\ s^{-1}$ are shown, covering the regimes of creep, quasi-static, dynamic, and impact, each with their respective mechanical test apparatus. This work covers strain rates ranging from quasi-static to dynamic, where it is distinguished between intermediate and high strain rates.

into account, which are required to draw conclusions on energy absorption.[11,12,21] Other studies look individually at quasi-static[3,6,8–10,14,15,22] or dynamic strain rates,[7,11] but do not provide information on the validity of the results outside these ranges.

While all of these studies contribute a great deal to the fundamental understanding of individual aspects in cellular structures, their biggest drawbacks are that they use different materials, different fabrication processes, different modeling procedures, different unit cell types, different relative densities, or other properties, which makes it hard to compare the results to one another in a systematic way.[3,8–10,14–17,22–24] Results that are more comparable and more generalizable are critically important for designers, engineers, and scientists, to take full advantage of the potential and create the most efficient parts.

Our work aims at accommodating all of these aspects in a single comprehensive study. Specifically, we compare various 3D lattice structures of unit cell types ranging from a connectivity, Z, of four, which is well within the bending dominated regime, to 14, which is well within the stretching dominated regime, in periodic tessellations of different build angles and in stochastic order, over a wide range of strain rates (**Figure 1**). The unit cells encompass Voronoi decomposition ($Z = 4$), cubic ($Z = 6$), octet-truss ($Z = 12$), and Delaunay triangulation ($Z = 14$) cells that are tested for orientation angles of $\alpha = 0^\circ, 15^\circ, 30^\circ, 45^\circ$ and compared to stochastic structures (**Figure 2**). The strain rates studied range from quasi-static, typically defined between $10^{-6}\ s^{-1}$ and $10^0\ s^{-1}$, to dynamic ranges of $10^4\ s^{-1}$, where rates between $10^0\ s^{-1}$ and $10^2\ s^{-1}$ are characterized as dynamic intermediate strain rates and rates between $10^2\ s^{-1}$ and $10^4\ s^{-1}$ as high strain rates (Figure 1). We choose aluminum as the constitutive material of the lattices in our computational model, to compare our findings to those reported in prior publications.[3,25–28]

First, we present an overview of the parameter space tested and the methodology used to generate and numerically test the structures. Detailed results are presented for all unit cell types and rotations as well as the stochastic structures for a strain rate of $100\ s^{-1}$. This includes stress–strain distributions as extracted from the numerical analyses, the resulting stress–strain curves, as well as overview graphs comparing the modulus and peak stress to the volumetric energy. In the final section, we present the effect of strain rate on the peak stress, energy absorption, and energy absorption per peak stress for all tested scenarios.

2. Experimental Section

2.1. Lattice Generation

Four different lattice topologies are considered, that is, Voronoi decomposition-based, cubic, octet-truss, and Delaunay triangulation-based, each categorized by their average number of connectivity, that is, 4, 6, 12, and 14, respectively. While Voronoi composition and Delaunay triangulation are means to generate different lattice topologies, their connectivity typically remains constant and, here, the focus is on this general case.[29] According to Maxwell's criterion, (3D) unit cells with a connectivity of $Z < 12$ are bending dominated and $Z \geq 12$ stretching dominated.[23] Of the four unit cell geometries, the octet-truss sufficiently satisfies the Maxwell criterion for rigidity and is topologically stretching dominated.[30–32] The cells generated using Voronoi decomposition and cubic cells are topologically bending dominated, space-filling polyhedra. The Delaunay triangulation generates a redundant structure and over-constrained, but also classified as topologically stretching dominated. The cross-sectional shapes of the struts in each lattice are circular with constant diameter.

Several rotated equivalents of the four different periodic lattices are simulated to check for the degree of anisotropy between each. The range of rotation angles are chosen such that the rotated lattice geometry is not redundant due to symmetry. All unit cell geometries have three fourfold symmetries, where a rotation of 90° with respect to those axes will result in the same geometry. All cells have at least three mirror symmetry planes. Thus, all the cells only need to be rotated up to 45° before they repeat themselves in a mirrored equivalent. For example, rotating the cubic lattice by +60° would be the same as rotating it by −30°.

In the scope of this work, both the Voronoi decomposition and the Delaunay triangulation use a body-centered cubic (BCC) point grid, generated periodically in 3D for the periodic structures.[29] The Delaunay-based lattices are generated by a triangulation of the points in a periodic point cloud.[33] The partitions of the Voronoi-based lattices are generated within a bounding box encompassing all points in the point cloud.[34] The edges of the partitions are extracted and defined as the struts of the lattice. The periodic cubic and octet lattices are generated by tessellating the respective unit cell in the three dimensions.

To rotate the lattices, their edges are rotated around the <0,1,0> axis. A bounding box of the desired dimensions is generated and all edges outside the box are trimmed. Struts that are smaller than a specified tolerance, that is, equal to the diameter of the strut, are merged. This is important for the simulations, to avoid disproportionately small characteristic element lengths that can be problematic for convergence. All struts that are not connected to the body of the lattice are deleted.

For stochastic lattices generated using Voronoi decomposition, the displacements of all points in the cloud are randomized

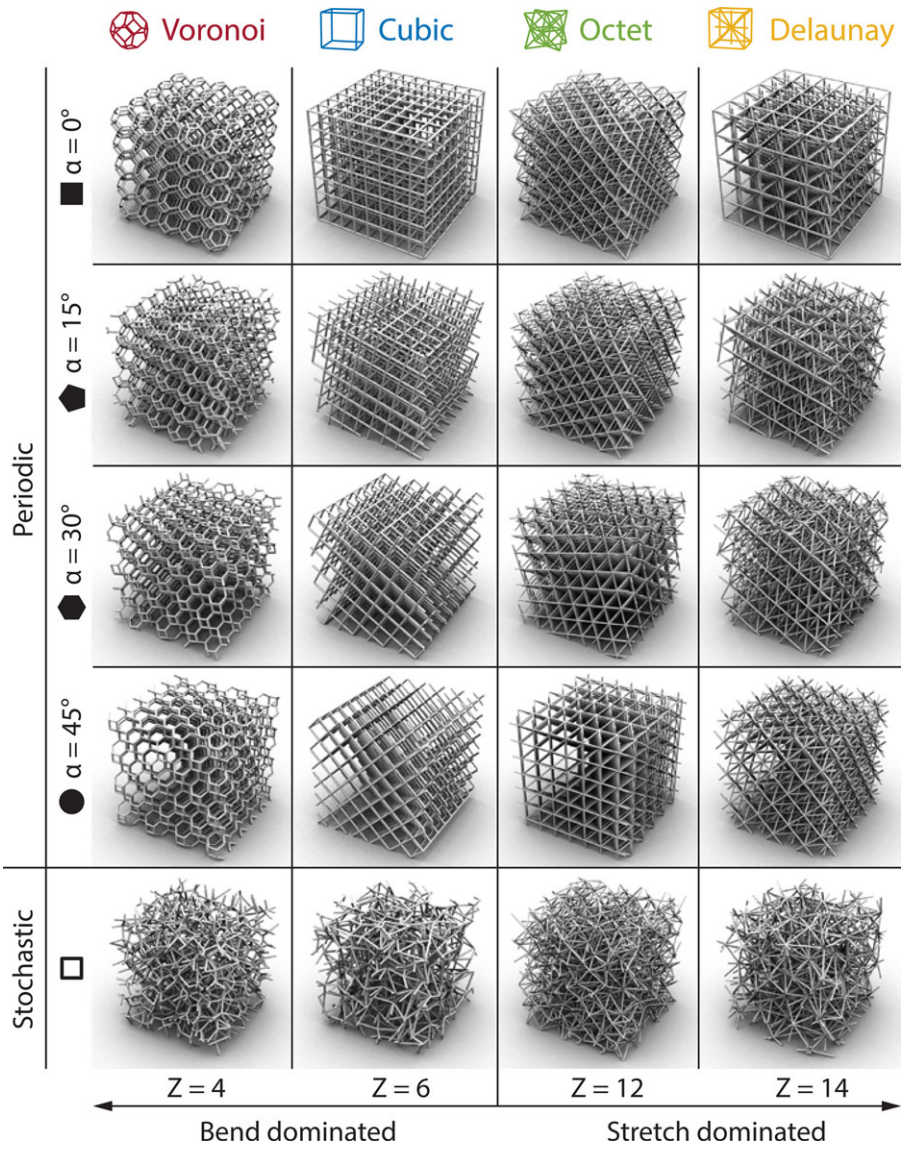

Figure 2. Test parameters and structures. Four different lattice types with unit cells of connectivity, Z, ranging from 4 (bending dominated) to 14 (stretching dominated) are investigated. For each structure, the effect of anisotropy is tested with periodic tessellations of load orientations, α, of 0°to 45°. Given by the unit cell architectures, this range covers all possible (in-plane) rotations, before the architecture repeats itself in a mirrored manner. Lastly, the stochastic counterparts with identical numbers of connectivity are investigated.

within a unit cube using weights as a scaling factor. Seed numbers are used to generate a pseudo-random set of perturbations from a continuous uniform distribution. This is to ensure that the same random lattice structures are reproducible. The randomization happens before the tessellation. The cell edges are always bending dominated and have a connectivity of four, that is, similar to the periodic versions. The only exception is when the tessellation points are aligned as a cubic grid, which yields a connectivity of six. For the stochastic lattices generated using Delaunay triangulation, the average connectivity of the structure is different for different sets of points. The average connectivity of a periodic BCC Delaunay triangulation is 14. To generate a stochastic structure with the same connectivity, the vertices of the triangulated lattices are displaced randomly. The same procedure is used for the stochastic equivalents of the cubic and octet-truss lattices. The stochastic equivalents are not rotated since it is assumed that stochastic foams are (quasi-)isotropic and rotating a random geometry would yield another random geometry.[35–37]

For the final design of the lattices, there are no boundary faces along the surface of a bounding box for any lattice structure, that is, the struts that are trimmed at the bounding box surface are not connected to one another. This is common practice in literature since the number of interior cells would be sufficient to characterize the structure and any boundary effects would be minimized.[3,6,9,16] This is also similar to mechanical testing of

open and closed cell foams where the experimenter would simply cut a specimen out of the bulk material.

2.2. Energy Absorption and Peak Stress

For this study, two main mechanical behaviors are investigated: the energy absorption of the lattice to a specified strain and the peak stress. The absorbed energy, U, is the strain energy of the lattice, defined as the area under the stress–strain curve

$$U = \int_{\varepsilon_i}^{\varepsilon_f} \sigma(\varepsilon)\, d\varepsilon \tag{1}$$

where $\varepsilon_i = 0$ and $\varepsilon_f = 0.80$. By integrating the stress–strain curve, the energy is a volumetric measure independent of the size of the lattice. This volumetric energy provides insight as to the amount of dissipated energy due to different lattice deformation modes.

An additional measure of how an energy absorbing structure performs is the peak stress, which for this study, amongst others, will be defined as the transmitted stress that initiates crushing of the lattice. The peak stress is important when designing protective liners because this is the stress transmitted to the protected item. As shown by Gibson and Ashby, these two measures are important for designers in selecting the appropriate foam properties for a specific application.[38]

2.3. Simulation

Abaqus/Explicit is used and all simulations are run on the ETH Euler high-performance computing cluster utilizing a maximum of 48 cores, with 8 cores and 2048 megabytes of ram per core dedicated to each simulation. The lattices are strained to a maximum of 80% for the energy absorption calculations and 3% for the stiffness and peak stress calculations to have a higher resolution,

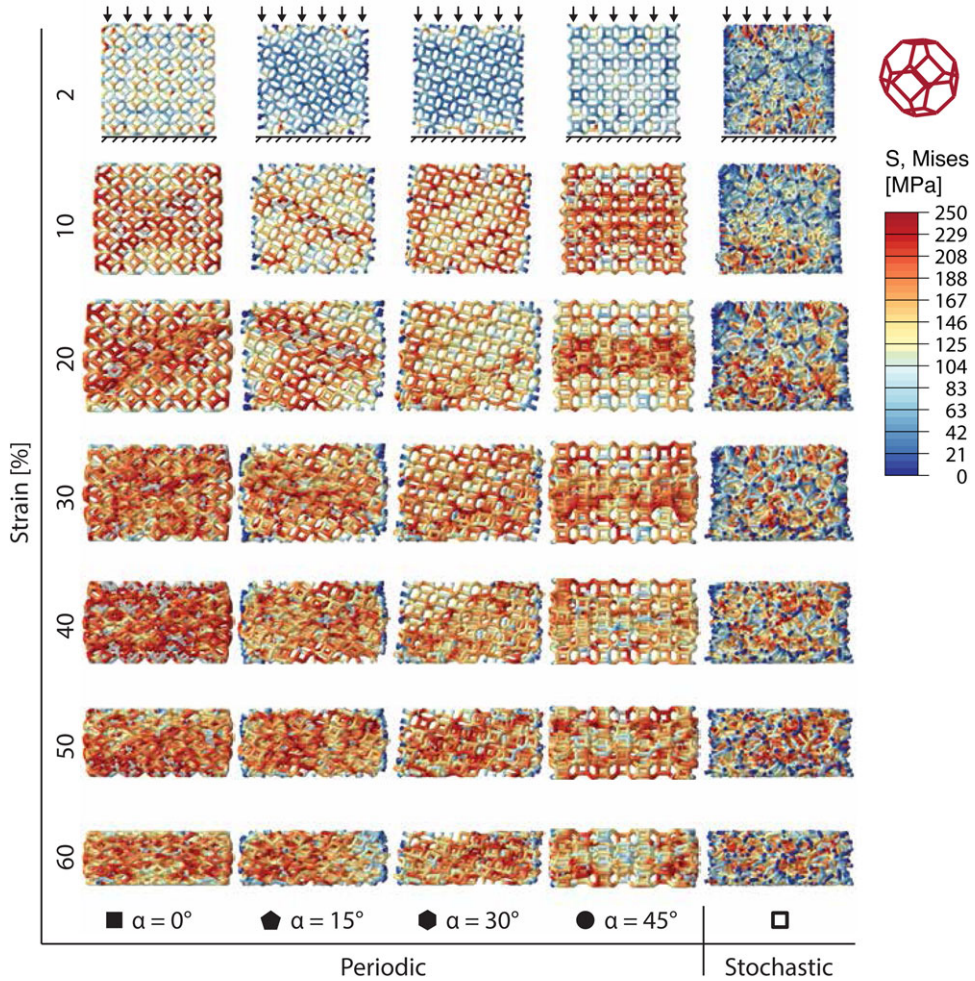

Figure 3. Stress distribution of Voronoi-based structures ($\dot{\varepsilon} = 10^2\ s^{-1}$). A front view of the von Mises stress distribution on straining the Voronoi unit cell based lattices is shown for a strain rate of $\dot{\varepsilon} = 10^2\ s^{-1}$. The structures are strained in compression between two solid plates and the results are shown for all periodic load orientations as well as their stochastic counterpart. A diagonally layer-wise failure of different degrees is seen for all but the stochastic structure, in which seemingly arbitrary struts are progressively loaded until failure. Generally, a large amount of struts is equally strained to almost the maximum, indicating a high plateau-strength without an initial peak stress.

with 600 data points recorded in each simulation. Strain rates are calculated based on the specimen dimensions as $\dot{\varepsilon}_t = v(t)/L_0$, where $v(t)$ is the difference in moving speed between the upper and lower plate, respectively, and L_0 the initial height of the specimens. Quadratic Timoshenko beam elements (Abaqus element type B32) with an approximate element length of 0.5 mm are used. This yields a different number of elements per strut, rather than a defined number of elements per strut, which is in accordance with prior work.[6,9] For any given lattice, it also yields at least three elements per strut, which has been found to be sufficient to accurately capture linear and non-linear responses as well as the failure behavior of struts.[6,9] However, it is important to note that the required number of elements and element size can be different for different strut aspect ratios, which range in this study from about 4 to 16. To accommodate nodal effects of the pin-jointed beams, the strut stiffness in vicinity of the nodes has been increased. The results are in good agreement with a solid model, both for low and high connectivities, but the overall effect is found to be minor, likely due to the relatively high aspect ratios of the struts. An element sensitivity analysis is carried out to ensure that the results are not sensitive to the element size. To maintain high accuracy across the different strain rates tested, no mass scaling is used.

Aluminum alloy Al-6101 T6 material is modeled, which is commonly used in literature to model Al foams and the constituent material of the commercially available Duocel foam.[3,25–28] The material model is linear elastic-plastic with damage evolution at a fracture strain of $\varepsilon_f = 19\%$ and, due to the strain-rate independence of Al-6101 T6, does not include strain rate effects. The elastic modulus is $E = 68.9$ GPa, the yield strength $\sigma_y = 193$ MPa, the ultimate tensile strength $\sigma_{\text{UTS}} = 221$ MPa, the Poisson's ratio of $\nu = 0.33$, and the density $\rho = 2.7$ g cm^{-3}. Numerous studies have shown a lack of significant strain rate effects, which allows us to isolate the effects of geometry at different strain rates.[21,39–42]

The lattice is placed between two steel plates of $E = 200$ GPa and $\rho = 8$ g cm^{-3}, one stationary (bottom) and one crush plate (top, Figure S1, Supporting Information). The plates are modeled with solid elements (Abaqus element type C3D8R) of size 2 mm. The stationary plate is constrained in all degrees of freedom. The crush plate is constrained in the in-plane degrees of freedom, X and Y. The velocity of the crush plate is kept constant throughout

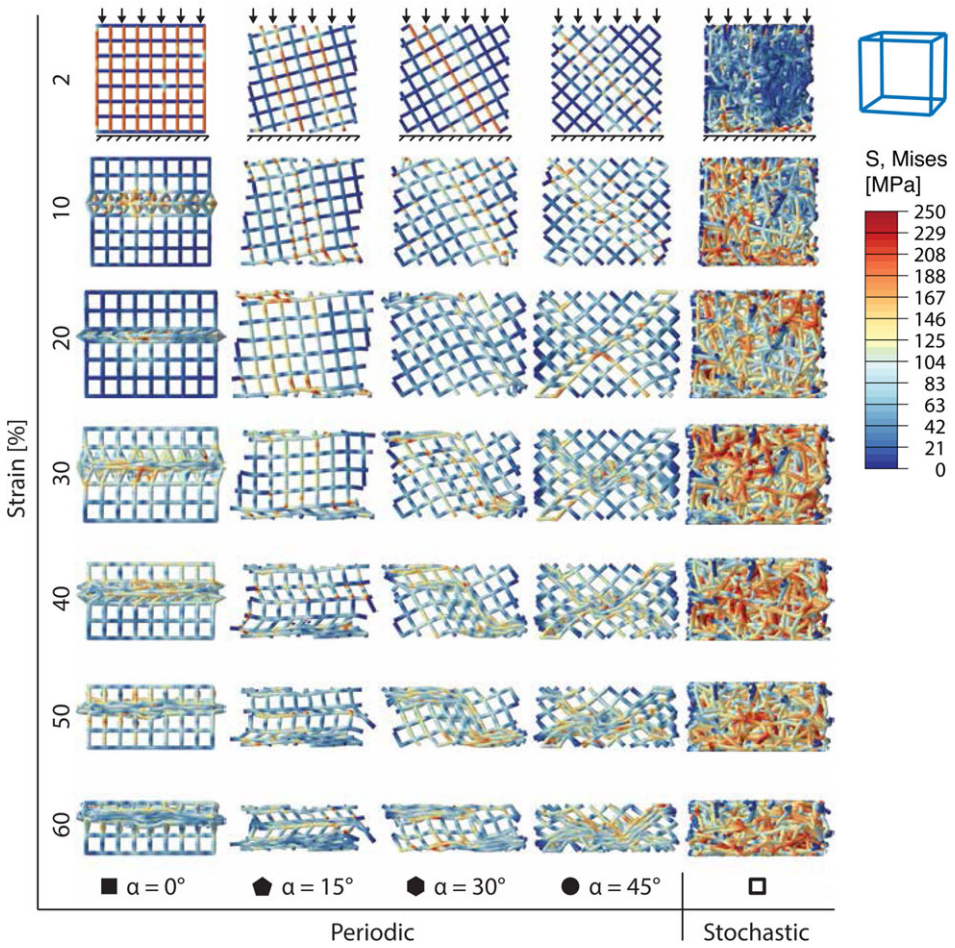

Figure 4. Stress distribution of cubic-based structures ($\dot{\varepsilon} = 10^2\ s^{-1}$). Von Mises stress distributions shown for different strain states of the cubic unit cell based geometries, again for a strain rate of $\dot{\varepsilon} = 10^2\ s^{-1}$. Large discrepancies are seen between the different orientations. While $\alpha = 0$ shows a high, uniform loading at 2% strain, which catastrophically fails right after, the other orientations, including the stochastic structure, shows a more uniform stress distribution across the different strains.

the entire simulation and selected based on the impact strain rate. Rotation boundary conditions for the top and bottom nodes of the lattice are constrained from rotating around the in-plane (*X, Y*) direction to reinforce the edges from local crushing at the top and bottom surface. This is to avoid local deformations from dominating the failure behaviors of the lattices, which is particularly important for the rotated and stochastic structures, that possess incomplete unit cells.[6,9] Reaction forces at the bottom plate are extracted to determine the mechanical response of the lattice.

The computational analysis incorporates self-contact of the beam elements and general contact between the lattice elements and that of the plate. All contacts use a penalty formulation. The coefficient of friction between the steel plate and the aluminum foam is set to $\mu = 0.61$.

3. Results and Discussion

The von Mises stress distribution is shown for different (global) strain levels of $\varepsilon = 2\%,\ 10\%,\ 20\%,\ 30\%,\ 40\%,\ 50\%,\ 60\%$ for the different orientations and stochastic version of the Voronoi structure (**Figure 3**). For $\alpha = 0^\circ$, it can be seen that, at lower strains, that is, strains of $\varepsilon = 10\% \ldots 20\%$, the highest stresses of about 250 MPa occur diagonally and crosswise, where whole unit cells, rather than individual struts, tend to have similar stresses. These layers initiate a layer-wise failure at strains $\varepsilon > 20\%$. Multiple collapses can be identified, potentially yielding local peaks in the stress-strain response. At $\alpha = 15^\circ$, a similar, crosswise stress distribution is seen that is rotated by 15° and less pronounced. No such stress distribution is seen at $\alpha = 30^\circ$, but is again seen at $\alpha = 45^\circ$, which also exhibits a layer-wise failure behavior. In the stochastic lattice, seemingly random struts are strained and fail individually at all strains tested. In all Voronoi periodic and stochastic lattices, the number of struts that are equally strained does not vary significantly throughout the strains shown, indicating that the load bearing capability does not significantly change. Hence, a plateau is expected in the resulting stress–strain curves within this range for all Voronoi-based lattices, up to the densification.

For the cubic unit cell structures, significant differences between the build orientations are observed (**Figure 4**). Specifically, at $\alpha = 0^\circ$ the vertical struts are almost uniformly strained to the

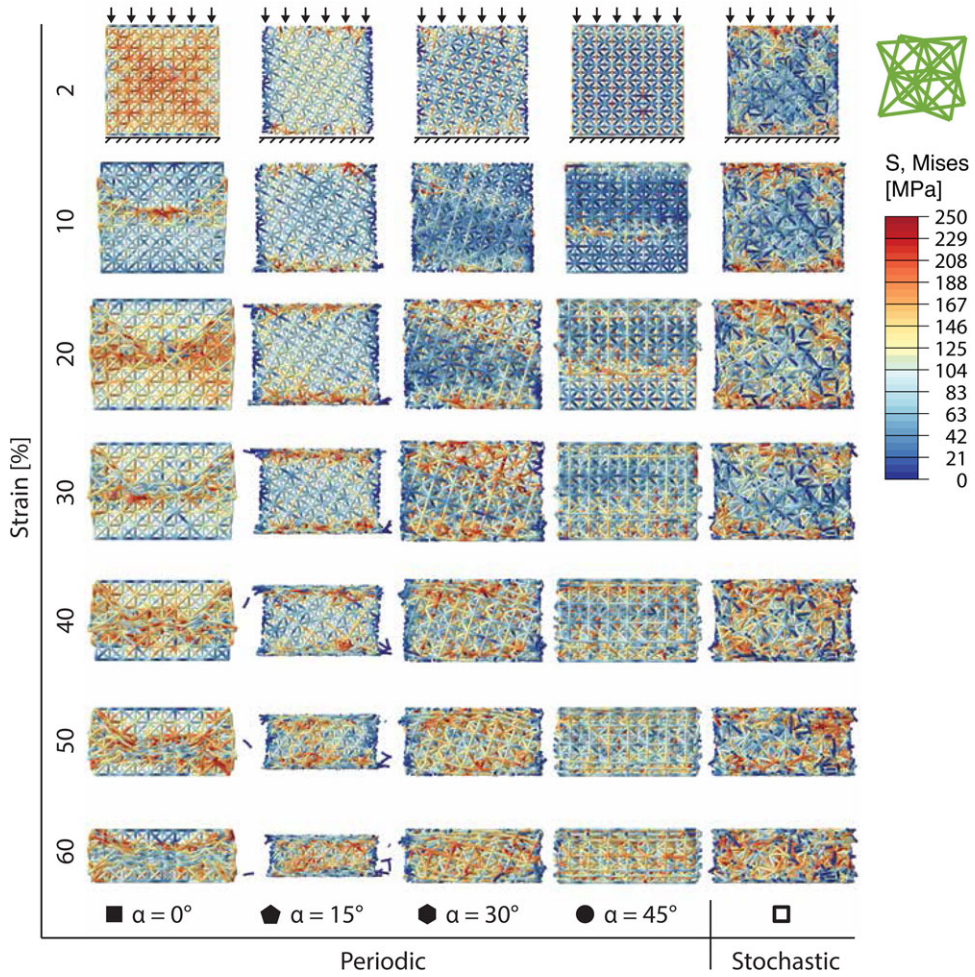

Figure 5. Stress distribution of octet-truss-based structures ($\dot{\boldsymbol{\varepsilon}} = 10^2\ \boldsymbol{s}^{-1}$). Front view of von Mises stresses plotted at different strains for the octet-truss based lattice, as obtained for a strain rate of $\dot{\varepsilon} = 10^2\ s^{-1}$. The uniformity of the stress distribution across different strain states is relatively high for all but the 0° and 15° rotations, indicating that these exhibit a stretching dominated behavior, that is, a large, initial peak stress followed by multiple peaks.

maximum observed von Mises stress of 250 MPa at small strain. At a strain of $\varepsilon = 10\%$, an internal horizontal layer fails completely, relaxing the other struts. This layer-wise failure repeats itself after strain increments equivalent to the unit cell height of the lattice until all layers have failed. This behavior implies a stretch-dominated lattice with a high, initial peak stress, followed by additional stress peaks due to the failure of each layer. The reasoning for a strong, layer-wise behavior is supported by the fact that the stress distribution, in particular, at low rotation angles, is non-uniform. For $\alpha = 15^\circ$, the struts tilted 15° from the vertical that touch both the top and bottom compression plates exhibit a similar, yet alleviated behavior as seen for $\alpha = 0^\circ$, likely due to the influence of the orthogonal struts and out-of-plane forces. Similar to $\alpha = 0^\circ$, a layer-wise failure is observed for $\alpha = 15^\circ$. However, instead of the middle layer failing first, the top and bottom layers now fail first, which are weakened by being incomplete layers, indicating that the initial peak stress should be significantly lower when compared to the $\alpha = 0^\circ$ lattice. The failures of the top and bottom layers also trigger the failures of the consecutive layers, again, indicating that the layer effects are alleviated. This trend continues at higher rotations of $\alpha = 30^\circ$ and $\alpha = 45^\circ$, where an even less pronounced layer-wise failure is observed. In fact, the failure modes for $\alpha = 45^\circ$ and the stochastic lattice are comparable to those of the Voronoi lattice, indicating a bending rather than stretching dominated failure mode, which we expect will result in a relatively constant plateau stress throughout the strain range.

The octet-truss lattice of $\alpha = 0^\circ$ shows a crosswise stress distribution (**Figure 5**), which is due to the absence of vertical struts in the unit cell. In contrast to the Voronoi lattice, the stress is distributed throughout the octet lattice already at $\varepsilon = 2\%$ and, on failure, the stresses become concentrated in the center of the structure ($\varepsilon = 10\%$), and then stress becomes more distributed again ($\varepsilon = 20\%$). This pattern repeats with increasing strain, indicating a non-uniform stress–strain curve with a pronounced initial peak followed by smaller peaks in the range of about the unit cell height. Octet-trusses rotated by $\alpha = 15^\circ$ show initial failure at the top and bottom layers, similarly to the same rotation of the cubic lattice, that continues spreading until densification is reached. No layer-wise failure of the internal

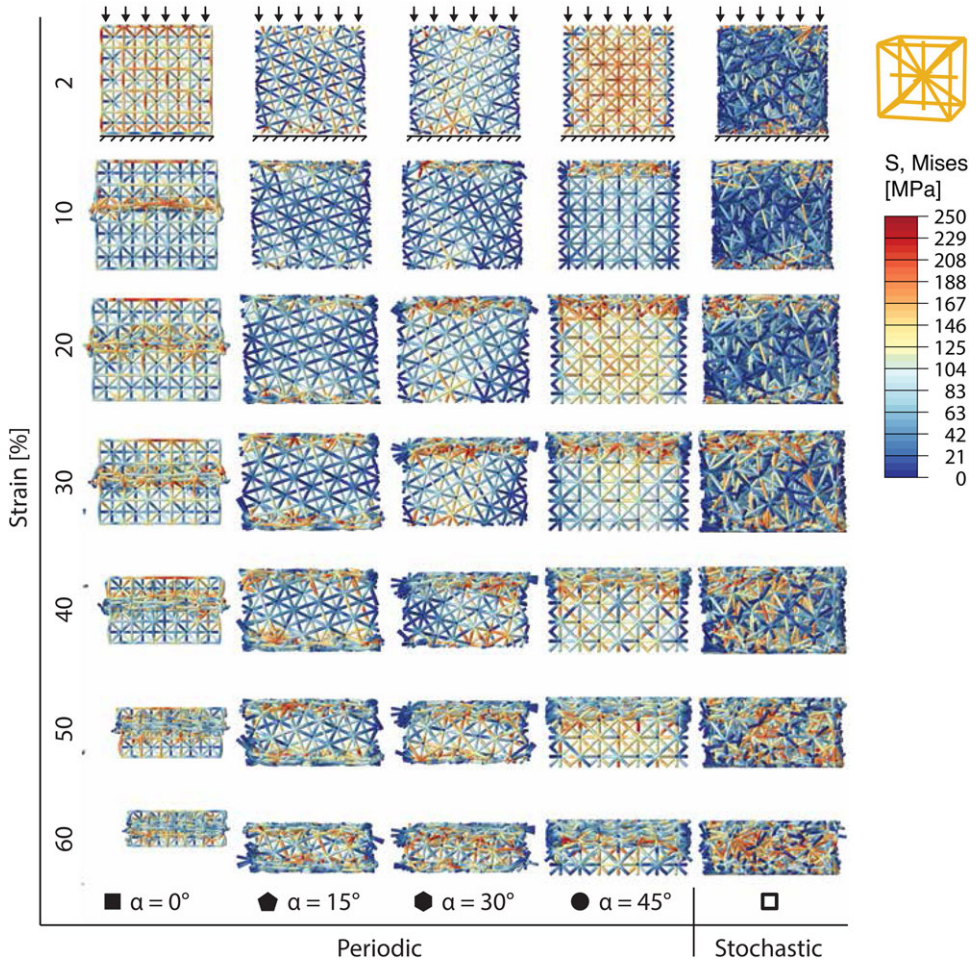

Figure 6. Stress distribution of Delaunay-based structures ($\dot{\boldsymbol{\varepsilon}} = 10^2\ s^{-1}$). The front view of the von Mises stress distribution is shown for the Delaunay based lattices tested at a strain rate of $\dot{\varepsilon} = 10^2\ s^{-1}$. A layer-wise failure is observed for $\alpha = 0^\circ$, where the inner layers fail first. This is in contradiction with the other orientations and the stochastic structure, where the top or bottom layers fail first due to partially incomplete unit cells. As the strain distribution varies across the different strains, a stretching dominated behavior is expected.

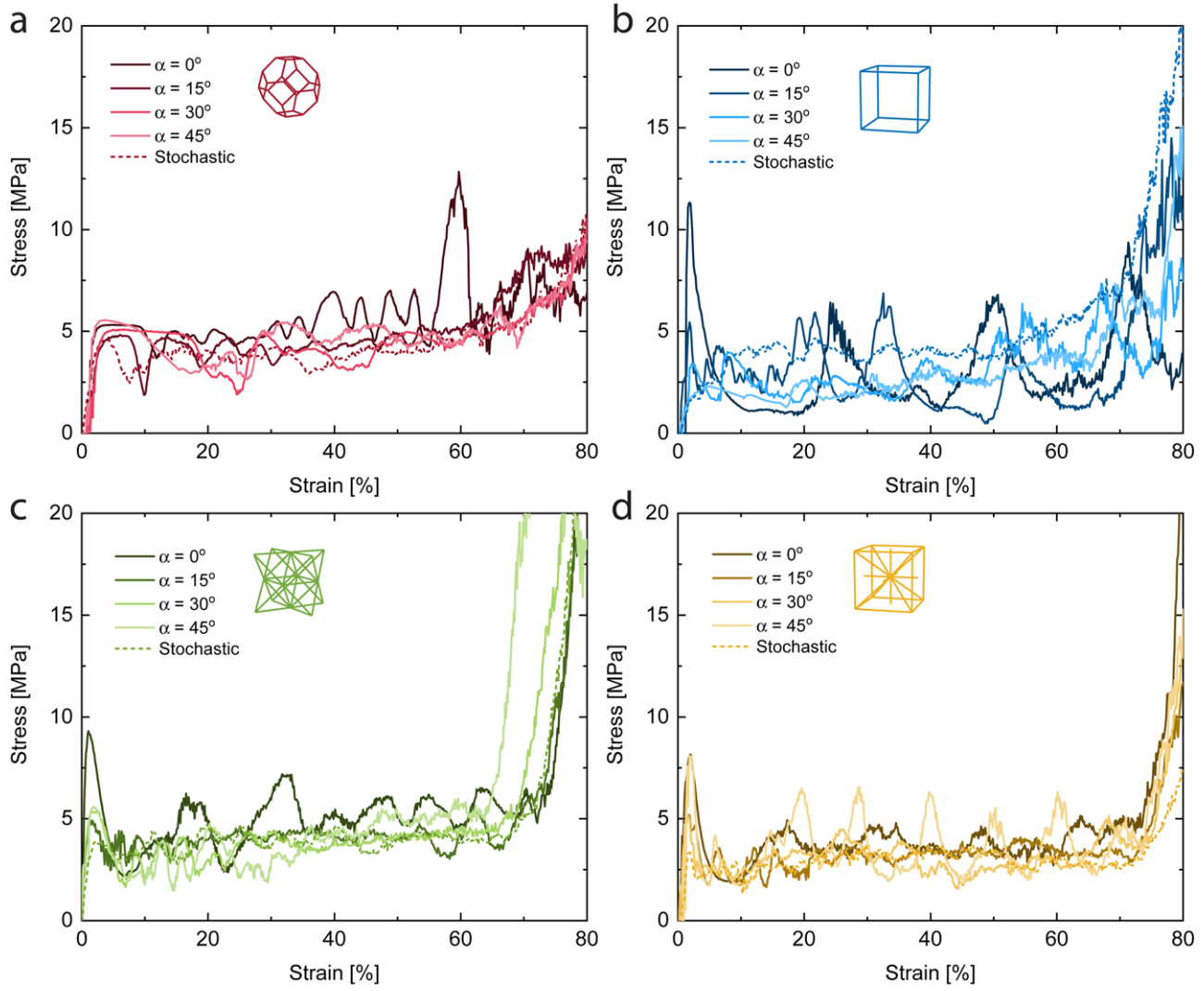

Figure 7. Stress–strain diagrams ($\dot{\varepsilon} = 10^2\ s^{-1}$). Stress-strain diagrams of the tested structures shown for a strain rate of $\dot{\varepsilon} = 10^2\ s^{-1}$. a) All Voronoi-based geometries show a typical bending dominated behavior, as characterized by little to no initial peak stress, followed by a relatively constant plateau. b) For the cubic based geometries, both bending and stretching dominated curves are found, depending on the unit cell orientation and periodicity. c,d) Both the periodic octet-truss and Delaunay triangulation show an initial peak stress followed by multiple minor peaks, a typical indicator for stretching dominated behavior. All stochastic structures exhibit bending dominated behavior, regardless of the unit cell type.

unit cells is observed. A layer-wise, yet less pronounced failure is observed again at $\alpha = 30^\circ$ and $\alpha = 45^\circ$, where individual elements are strained in tension, rather than compression, given by the unit cell geometry. Layer-wise failure is then observed along the longitudinal direction of these strained elements. The octet-based stochastic lattice shows stress concentrated on the top and bottom layers at small strains, which becomes more distributed through the lattice as strains increase.

The Delaunay cell-based structure consists of elements aligned at 0° and 45°. Due to the high connectivity, the whole $\alpha = 0^\circ$ and $\alpha = 45^\circ$ structures are stressed relatively uniformly at small strains with higher stresses at struts in the vertical direction (**Figure 6**). Similar to the cubic and octet-truss, the initial failure of the Delaunay lattice occurs at $\varepsilon = 10\%$, as opposed to the bending dominated Voronoi structure where it occurs in the range of $\varepsilon = 20\%$. The $\alpha = 15^\circ$ and $\alpha = 30^\circ$ Delaunay structures show increased stresses in the 15° rotated vertical elements with failure occurring predominantly at the top and bottom ends, similar to that of the rotated octet lattices. Similar behavior is observed in the Delaunay-based stochastic structure, which shows more members in the center failing throughout the strain range.

The resulting stress-strain curves corresponding to the deformation modes shown in Figures 2–5 are shown in **Figure 7** and generally are in good agreement with the qualitative observations made above. For the Voronoi structures (Figure 7a), typical bending dominated curves are observed for all rotation angles and the stochastic structure. Specifically, a relatively constant plateau of about $\sigma = 5$ MPa is reached without significantly higher peak stresses before densification sets in at higher strains, that is, at $\varepsilon > 60\%$.

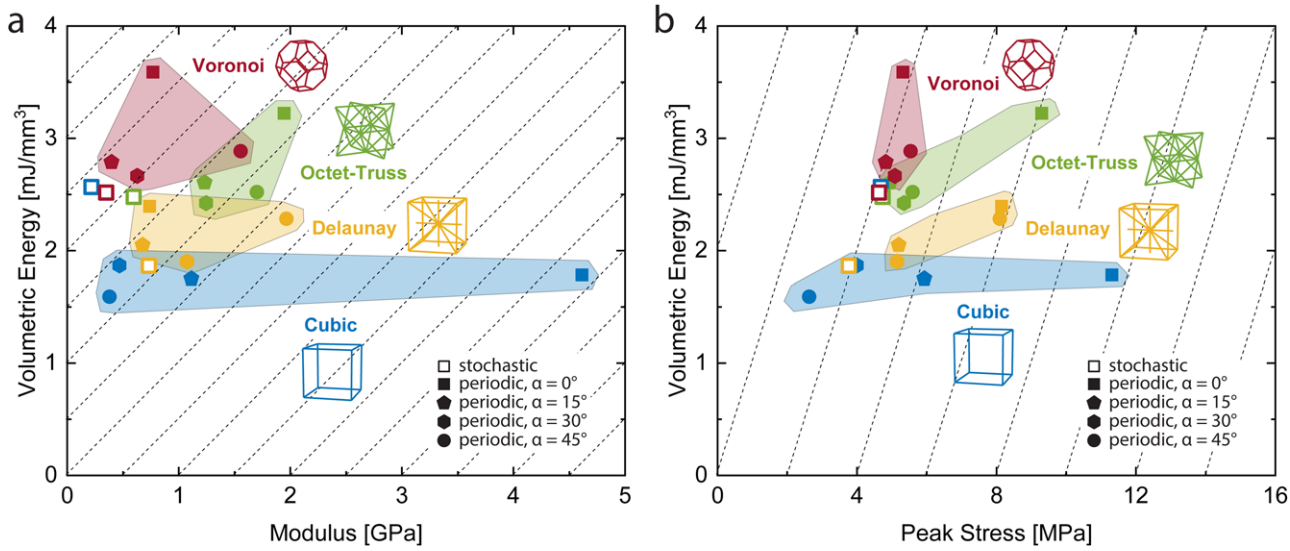

Figure 8. Modulus and peak stress versus volumetric energy ($\dot{\varepsilon} = 10^2\ s^{-1}$). As hypothesized from the stress distributions at different strain rates and observed in the stress-strain curves, large variations exist among different structures, periodicities, and unit cell orientations. a) shows the modulus plotted versus the volumetric energy, where the Voronoi-based and stochastic structures provide the lowest moduli to energy ratios, which is considered advantageous for, for example, protective equipment. Structures that are stiffer, tend to exhibit less energy absorption capability. b) Similar trends are seen for the peak stress versus volumetric energy ratio, where the Voronoi-based structures perform well. This is in accordance with literature, which consistently reports this unit cell to be the first choice in energy absorption applications. However, if this ratio is the only parameter of interest, the cubic cell at $\alpha = 45°$ performs even better. The dashed lines indicate constant volumetric energy versus modulus or peak stress ratios.

Large differences between the curves are found for the different rotation angles of the cubic structure (Figure 7b). Specifically, $\alpha = 0°$ shows a typical stretching dominated curve with a high initial peak stress of $\sigma = 11.5$ MPa, followed by multiple peaks separated by the layer height of the unit cells, in between which the load drops to $\sigma < 2$ MPa. A similar, yet smoother curve is seen for $\alpha = 15°$, where the initial peak stress reaches $\sigma = 5$ MPa, followed by peaks of about the same height, and valleys of about $\sigma = 3$ MPa. The structures with $\alpha = 30°$ and $\alpha = 45°$, and the stochastic structures show a typically bending dominated behavior with no initial peak and a plateau height of around $\sigma = 3$ MPa. The sensitivity to the load orientation is in accordance with existing literature.[43,44] The energy absorption, that is, area under the stress–strain curve, is generally lower than those of the Voronoi structures.

The octet-truss shows pronounced differences between the different rotation angles (Figure 7c), similar to the cubic unit cell. At $\alpha = 15°$, an initial peak stress of $\sigma = 9.4$ MPa is observed followed by peaks of around $\sigma = 6$ MPa and valleys of $\sigma = 4$ MPa. The other orientations and the stochastic structures show no significant initial peak and the stress plateaus around $\sigma = 4\ MPa$.

The Delaunay based structures show a stretching dominated behavior throughout the different unit cell orientations, with peak stresses ranging from $\sigma = 5 \ldots 8$ MPa and valley stresses down to $\sigma = 2$ MPa.

In summary, the largest differences due to orientation and periodic lattices versus stochastic lattices are seen for the cubic structure, followed by the octet-truss and Delaunay structure both for the modulus and peak stress (**Figure 8**). The Voronoi structure shows a relatively consistent behavior across these parameters, which is the reason it is commonly used for energy absorbing applications, where an optimization for unit cell orientation is not feasible. When relating the peak stress to the volumetric energy, however, the $\alpha = 45°$ orientation of the cubic lattice outperforms all Voronoi structures (Figure 8b). This is particularly interesting for parts and structures where efficiency is important and load orientation is known a priori. The stochastic structures of all unit cell types show essentially the same modulus and peak stress ranges, with the exception of the Delaunay structure, which exhibits slightly smaller volumetric energy values. These findings are in accordance with literature, which states that, for stochastic structures, the relative density is the key tuning parameter.[23] Local and global buckling, which occurs predominantly in stretching-dominated regimes, is an additional factor of influence for the described energy absorption behaviors.

Besides the results presented in detail for a strain rate of 100 s^{-1}, the study is also conducted for lower and higher strain rates, $\dot{\varepsilon}$, ranging from 1 to 10 000 s^{-1} in step sizes of one decade (**Figure 9**). As for the peak stress, there is a little to no change at quasi-static and intermediate strain rates of $\dot{\varepsilon} = 1 \ldots 100\ s^{-1}$ (Figure 9a). At high strain rates, in particular, at $\dot{\varepsilon} = 10\ 000\ s^{-1}$, a sharp increase in the peak stress is observed for all but the Voronoi-based structures, which generally seem to be unaffected by the strain rate range tested. This has also been seen in previous work, where an increase in the initial peak stress has only been seen at the top, that is, crush, side of the structure, but not at bottom the support surface.[45] However, in these results, we show this can also occur at the bottom or transmitted surface. The increase has been attributed to the impact velocity of the compression plates, creating a transition or shock mode.[38] The energy absorption includes both elastic and plastic contributions (Equation (1)), and increases with increasing strain rate up to the strain rate of $\dot{\varepsilon} = 10\ 000\ s^{-1}$ (Figure 9b). This is also the strain

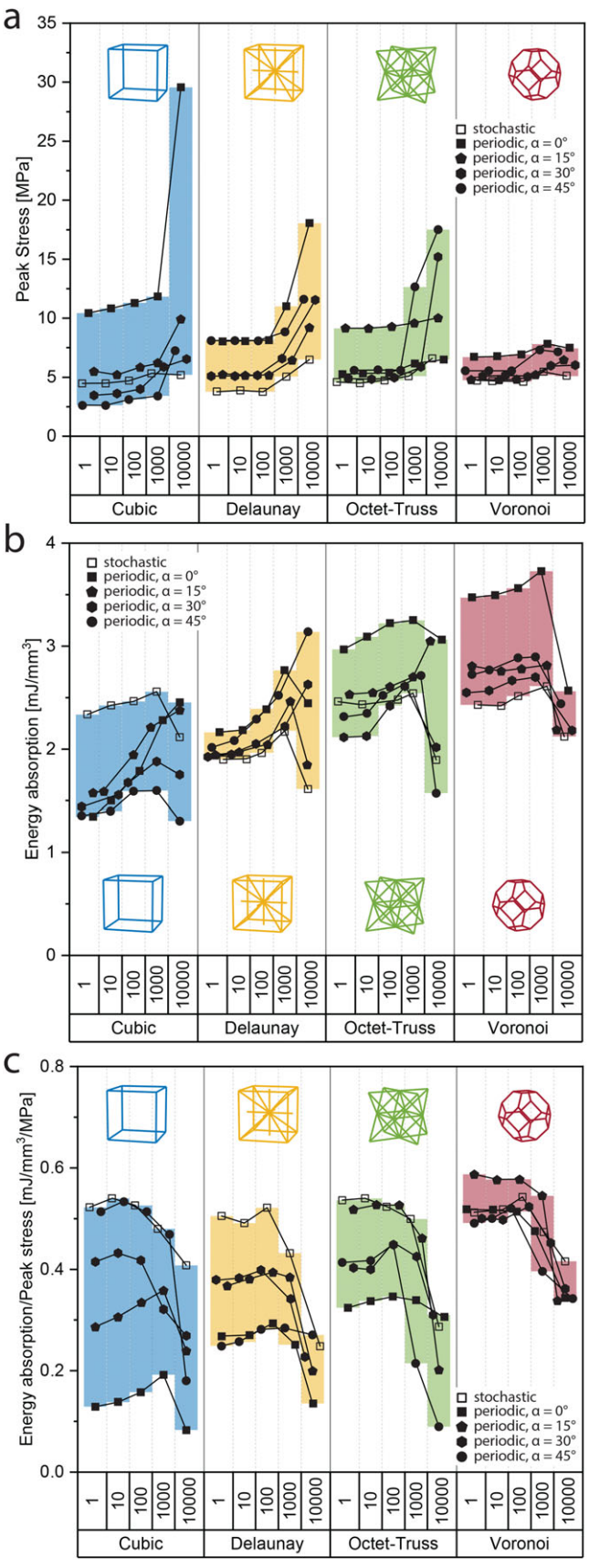

rate where the peak stress increases significantly and where dynamic effects, that is, transition or shock mode, set in. For the bottom plate, this means that the top plate is crushing the lattice at a rate faster than the shock wave, such that the impacting plate reaches the subsequent layers of the lattice first, hence the drop in energy absorption. Similar trends are observed for the effective energy absorption to peak stress ratio, which increases with increasing strain rate until it reaches the highest strain rate of $\dot{\varepsilon} = 10\,000\ s^{-1}$. Due to the strain-rate independence, the material Al-6101 T6 is used. All strain rate effects are expected to be due to inertia.

4. Conclusions

Here we present the first comprehensive study that compares the full deformation behavior of unit cells in 3D periodic with stochastic lattices with connectivities ranging from 4 to 14 under identical, experimental conditions. Specifically, the results confirm that relative density is the main tuning parameter for stochastic foams and that the deformation mode is the dominant parameter for periodic structures.[23,46] However, it is found that the energy absorption properties not only depend on the nodal connectivity, but also on the unit cell geometry and, in particular, the orientation of the load, which has been demonstrated before on individual unit cells.[44,47] For example, a cubic unit cell, which is defined as bending dominated according to its connectivity, can exhibit stretching dominated behavior when loaded along the horizontal or vertical directions. Further, it is found that the energy absorption properties for quasi-static strain rate loadings are generally applicable to low and intermediate strain rates. At higher strain rates, the absolute performance of the lattices drops significantly and their performance with respect to the load orientations changes. While the results cover a wide range of discrete, 3D, and open-cell lattices, it is not easily possible to compare the performance of all possible variations. For example, multi-stable materials can provide higher energy absorption than lattices, whereas lattices can outperform multi-stable materials in quasi-static conditions. Here, we focus on the study of lattices envisioning them to be more applicable in scenarios where specific load-bearing, static stiffness, and energy absorption properties are desired. However, the methodology can be extended to other classes of lattice materials that, for example, are 2D (honeycombs) or rely on (elastic) buckling or cell wall bistability.[48–50]

The large variability in the resulting dynamic properties of 3D unit cells and cellular structures due to the different parameters highlights the potential for lattice structures to be optimized for energy absorption properties. Specifically, cellular structures

Figure 9. Strain rate effect. The effect of strain rate on the mechanical properties is shown for the periodic and stochastic lattices. a) At strain rates between $\dot{\varepsilon} = 10^0 \ldots 10^3\ s^{-1}$, all structures are relatively insensitive to the strain rate. Depending on the build orientation, the Delaunay and octet-truss show a significantly increased peak stress at higher strain rates. b) A mixed effect is seen for the energy absorption, where the build orientation seems to have a stronger effect on the energy absorption than the unit cell type. c) The ratio between the two previously reported values shows a general decrease at strain rates of $\dot{\varepsilon} > 10^2\ s^{-1}$.

monolithically composed of identical unit cells can be optimized to maximize the performance, but further steps, such as combinations of unit cells, load orientations, and combining periodic with stochastic microstructures, can unlock unprecedented potential. The knowledge acquired in this comprehensive study can play a significant role in exploiting this potential for a wide range of applications, ranging from protective packaging of delicate components to crash and blast mitigation in automotive and aerospace structures, as well as multifunctional applications in biomimetic structures.

Supporting Information

Supporting Information is available from the Wiley Online Library or from the author.

Acknowledgements

The authors acknowledge Cynthia Tan for her early contributions to this work. The authors further acknowledge Jonas Schwarz for his contributions to the model used for the simulations in this work. This work was partially supported by an ETH Postdoctoral Fellowship to K.H.M.

Conflict of Interest

The authors declare no conflict of interest.

Keywords

architected structures, cellular solids, energy absorption, fracture, lattice structures

Received: April 24, 2019
Revised: July 6, 2019
Published online:

[1] J. Mueller, K. Shea, *Extreme Mechanics Letters* **2018**, *25*, 7.
[2] J. Mueller, J. R. Raney, D. M. Kochmann, K. Shea, *Adv. Sci.* **2018**, *5*, 1800728.
[3] M. Alkhader, M. Vural, *Int. J. Eng. Sci.* **2008**, *46*, 1035.
[4] J. Hawreliak, J. Lind, B. Maddox, M. Barham, M. Messner, N. Barton, B. Jensen, M. Kumar, *Sci. Rep.* **2016**, *6*, 28094.
[5] H. Jeon, J. R. Gross, S. Estabrook, S. Koumlis, Q. Wan, G. R. Khanolkar, X. Tao, D. M. Mensching, E. J. Lesnick, V. Eliasson, *Aerospace* **2015**, *2*, 353.
[6] M. J. Silva, L. J. Gibson, *Int. J. Mech. Sci.* **1997**, *39*, 549.
[7] Y. Liu X.-C. Zhang, *Explosion Shock Waves* **2008**, *6*, 002.
[8] M. Alkhader, M. Vural, *Acta Mater.* **2009**, *57*, 2429.
[9] M. J. Silva, W. C. Hayes, L. J. Gibson, *Int. J. Mech. Sci.* **1995**, *37*, 1161.
[10] S. D. Papka, S. Kyriakides, *J. Mech. Phys. Solids* **1994**, *42*, 1499.
[11] Z. Zheng, J. Yu, J. Li, *Int. J. Impact Eng.* **2005**, *32*, 650.
[12] A. Ajdari, H. Nayeb-Hashemi, A. Vaziri, *Int. J. Solids Struct.* **2011**, *48*, 506.
[13] J. Mueller, J. R. Raney, K. Shea, J. A. Lewis, *Adv. Mater.* **2018**, *30*, 1705001.
[14] V. S. Deshpande, N. A. Fleck, M. F. Ashby, *J. Mech. Phys. Solids* **2001**, *49*, 1747.
[15] M. Laroussi, K. Sab, A. Alaoui, *Int. J. Solids Struct.* **2002**, *39*, 3599.
[16] W.-Y. Jang, A. M. Kraynik, S. Kyriakides, *Int. J. Solids Struct.* **2008**, *45*, 1845.
[17] W.-Y. Jang, S. Kyriakides, A. M. Kraynik, *Int. J. Solids Struct.* **2010**, *47*, 2872.
[18] T. Stanković, J. Mueller, P. Egan, K. Shea, *J. Mech. Design* **2015**, *137*, 111405.
[19] T. Stankovic, J. Mueller, K. Shea, Optimization for Anisotropy in Additively Manufactured Lattice Structures, presented at *ASME Computers and Information in Engineering Conference*, **2016**.
[20] T. Stanković, J. Mueller, K. Shea, *Addit. Manuf.* **2017**, *17*, 67.
[21] P. J. Tan, S. R. Reid, J. J. Harrigan, Z. Zou, S. Li, *J. Mech. Phys. Solids* **2005**, *53*, 2206.
[22] J. Mueller, K. Shea, *Mater. Today Commun.* **2018**, *17*, 69.
[23] V. Deshpande, M. Ashby, N. Fleck, *Acta Mater.* **2001**, *49*, 1035.
[24] S. Xu, J. Shen, S. Zhou, X. Huang, Y. M. Xie, *Mater. Des.* **2016**, *93*, 443.
[25] W.-Y. Jang, S. Kyriakides, *Int. J. Solids Struct.* **2009**, *46*, 635.
[26] K. A. Dannemann, J. Lankford Jr, *Mater. Sci. Eng., A* **2000**, *293*, 157.
[27] J. Yu, X. Wang, Z. Wei, E. Wang, *Int. J. Impact Eng.* **2003**, *28*, 331.
[28] L. Gibson, *Annu. Rev. Mater. Sci.* **2000**, *30*, 191.
[29] A. Okabe, B. Boots, K. Sugihara, S. N. Chiu, *Spatial tessellations: Concepts and Applications of Voronoi Diagrams*, Vol. *501*, John Wiley & Sons, Weinheim **2009**.
[30] J. C. Maxwell, *The London, Edinburgh, Dublin Philosoph. Mag. J. Sci.* **1864**, *27*, 294.
[31] C. Calladine, *Int. J. Solids Struct.* **1978**, *14*, 161.
[32] S. Pellegrino, C. R. Calladine, *Int. J. Solids Struct.* **1986**, *22*, 409.
[33] D.-T. Lee, B. J. Schachter, *Int. J. Comp. Inf. Sciences* **1980**, *9*, 219.
[34] S. Fortune, in *Computing in Euclidean Geometry*, World Scientific, Singapore **1995**, p. 225.
[35] X. Zheng, H. Lee, T. H. Weisgraber, M. Shusteff, J. DeOtte, E. B. Duoss, J. D. Kuntz, M. M. Biener, Q. Ge, J. A. Jackson, S. O. Kucheyev, N. X. Fang, C. M. Spadaccini, *Science* **2014**, *344*, 1373.
[36] V. Deshpande, N. Fleck, *J. Mech. Phys. Solids* **2000**, *48*, 1253.
[37] M. Vural, *Dynamic Response and Failure of Cellular Networks*, In International Conference on Fracture (ICF11), Turin, Italy **2005**.
[38] L. J. Gibson, M. F. Ashby, *Cellular Solids: Structure and Properties*, Cambridge University Press, Oxford **1999**.
[39] Y. Chen, A. Clausen, O. Hopperstad, M. Langseth, *Int. J. Solids Struct.* **2009**, *46*, 3825.
[40] E. Semb, *Behavior of aluminum at elevated strain rates and temperatures*, Master's thesis, NTNU – Trondheim **2013**.
[41] L. D. Oosterkamp, A. Ivankovic, G. Venizelos, *Mater. Sci. Eng., A* **2000**, *278*, 225.
[42] V. Deshpande, N. Fleck, *Int. J. Impact Eng.* **2000**, *24*, 277.
[43] D. D. Symons, N. A. Fleck, *J. Appl. Mech.* **2008**, *75*, 051011.
[44] Y. Gan, C. Chen, Y. Shen, *Int. J. Solids Struct.* **2005**, *42*, 6628.
[45] Y. Liu, J. Yu, Z. Zheng, J. Li, *Int. J. Solids Struct.* **2009**, *46*, 3988.
[46] M. F. Ashby, T. Evans, N. A. Fleck, J. Hutchinson, H. Wadley, L. Gibson, *Metal Foams: a Design Guide*, Elsevier, New York **2000**.
[47] R. Biagi, H. Bart-Smith, *Int. J. Solids Struct.* **2007**, *44*, 4690.
[48] S. Shan, S. H. Kang, J. R. Raney, P. Wang, L. Fang, F. Candido, J. A. Lewis, K. Bertoldi, *Adv. Mater.* **2015**, *27*, 4296.
[49] B. Haghpanah, L. Salari-Sharif, P. Pourrajab, J. Hopkins, L. Valdevit, *Adv. Mater.* **2016**, *28*, 7915.
[50] D. M. Correa, C. C. Seepersad, M. R. Haberman, *Integr. Mater. Manufact. Innov.* **2015**, *4*, 10.